Journal of Highway and Transportation Research and Development (English Edition)
Open Access | Editor-in-Chief: Wanheng Li, Daming Lin | ISSN 2095-6215

J. highw. transp. res. dev.
https://doi.org/10.26599/HTRD.2026.9480122
Article Type: Research Article

Autonomous Collision Avoidance for eVTOL in Air-Ground Coordination Based on Rule-Constrained Dynamic Velocity Obstacle

Yuetan Zhang[1,*], Honghai Zhang[1,**], Wei Pan[1], Yulin Yuan[2]

[1] *College of Civil Aviation, Nanjing University of Aeronautics and Astronautics, Nanjing, Jiangsu 210016, China*

[2] *Nanjing Tiancheng Transportation Research Institute Company Limited, Nanjing, Jiangsu 211500, China*

*Email: Yuetan Zhang, zhang23@nuaa.edu.cn
**Corresponding author: Honghai Zhang, honghaizhang@nuaa.edu.cn

Received: date(30-Oct-2026); Accepted: date(04-Nov-2026)

Just Accepted

Abstract: Autonomous collision avoidance for electric vertical takeoff and landing (eVTOL) aircraft in structured urban low-altitude airspace must satisfy both physical collision-prevention requirements and operational rules. This study proposes a rule-constrained dynamic velocity vector optimization (RC-DVVO) framework. First, urban low-altitude operational rules, including no-fly zones, flight corridors, altitude layers, and speed limits, are decomposed and mapped into a time-varying rule-feasible domain in velocity space. Second, this domain and the kinematically executable domain are incorporated into a three-dimensional dynamic velocity obstacle model, with collision probability and time to collision used to construct a risk term. Neighboring aircraft intentions and ground-recommended velocities are then integrated into a multi-objective cooperative optimization model, which is solved in real time using rule-based pruning, risk prediction, and local continuous optimization. Simulations of multiple crossing conflicts in an urban canyon show that RC-DVVO achieves a collision-avoidance success rate of 99%, a rule-violation rate of 0.8%, a mean curvature of 0.0132 rad/m, and a mean decision time of 12.3 ms. Compared with classical DVVO, the success rate increases by 5 percentage points, the rule-violation rate decreases by 88.9%, and the mean curvature decreases by 28.6%, while the decision time meets the requirements of 20 Hz control. These results indicate that the method enables safe and smooth autonomous eVTOL collision avoidance within modeled compliance boundaries and provides a basis for incorporating computable rules into collision-avoidance decisions in low-altitude intelligent networks.

Keywords: electric vertical takeoff and landing aircraft; dynamic velocity obstacle; autonomous collision avoidance; air-ground coordination

1 Introduction

Continued urbanization has intensified road congestion, reduced commuting efficiency, and increased pressure to limit carbon emissions in megacities. Conventional two-dimensional ground transportation is increasingly constrained in its ability to support future demand for high-density, efficient, and low-carbon three-dimensional mobility. Urban air mobility (UAM) has emerged in response and is regarded as a new direction in transportation development following road, rail, and civil aviation. Its central objective is to use low-altitude urban airspace for safe, efficient, and automated passenger and cargo transportation within cities and urban agglomerations [1]. Electric vertical takeoff and landing (eVTOL) aircraft, which combine vertical takeoff and landing, electric propulsion, low noise, and maneuverability, are a promising vehicle platform for UAM. Conflict detection and resolution (CD&R) is a core component of autonomous eVTOL flight: its performance directly affects operational safety and airspace utilization and is essential to large-scale commercial deployment.

Urban low-altitude environments impose demanding requirements on eVTOL CD&R because they are highly dynamic, complex, dense, and constrained [2]. Buildings, cranes, and power lines restrict maneuvering space and require precise avoidance actions. Multiple types of eVTOL aircraft may cruise, turn, and climb concurrently in narrow airspace, creating intersecting trajectories and potentially cascading collision risks. To maintain order and efficiency, aircraft must comply with structured operational requirements, including altitude layers, speed intervals, and flight corridors [3]. Avoidance maneuvers must therefore remain compatible with these rules. Moreover, conflicts in large-scale operations can arise suddenly, and ground-based control alone cannot meet millisecond-level decision requirements, motivating frameworks that jointly integrate strategic route guidance with real-time, distributed collision avoidance [4]. Onboard autonomous navigation and air–ground coordination, as demonstrated in recent collaborative air-ground robotic systems, are needed to close the perception-decision-control loop [5,6,7].

Aircraft collision-avoidance methods are generally divided into planning-based and reactive approaches, both of which have exhibited limitations when validated against realistic UAM operational scenarios [8]. Planning-based approaches, represented by rapidly exploring random trees (RRT) and their variants, generate collision-free paths in advance. However, their limited adaptability to dynamic environments makes rapid responses to unexpected aircraft trajectory changes difficult, restricting their use primarily to static or slowly changing airspace [9]. Reactive approaches, including artificial potential fields (APF) and velocity obstacles (VO), use current environmental observations to respond to conflicts and generate avoidance actions. They are therefore better suited to dynamic UAM scenarios. In particular, VO methods construct collision cones in velocity space to efficiently identify avoidance velocities and have been widely applied to the collision avoidance of unmanned aerial and aquatic vehicles [10,11,12]. Although previous studies have incorporated aircraft kinematic constraints and improved collision-cone construction to enhance efficiency and smoothness in UAM-specific settings [13,14], many approaches still emphasize geometric collision avoidance while overlooking operational rules in structured airspace. This limits their alignment with practical UAM requirements.

Just Accepted

In practical UAM operations, eVTOL aircraft must follow fixed flight corridors, altitude layers, and other structured requirements rather than operate in unrestricted free flight. Avoidance actions that prevent physical collisions but violate airspace rules can disrupt traffic organization and introduce additional conflicts, reducing overall efficiency. A central challenge is therefore to incorporate urban low-altitude operational rules into VO decision-making so that physical collision avoidance and rule compliance are addressed together. This study investigates that challenge by modifying conventional VO methods for structured airspace and developing an autonomous conflict-avoidance framework better aligned with UAM operating conditions.

1.1 Related Work

1.1.1 Geometric Collision Avoidance

Geometric collision-avoidance methods have attracted considerable attention in robotic motion planning because of their intuitive mathematical formulation and computational efficiency. The velocity obstacle (VO) method was introduced by Fiorini and Shiller in 1998 [15]. It defines the set of velocities that lead to collision and selects a velocity outside that set. This provides a velocity-space formulation of motion planning in dynamic environments. However, the original VO method assigns the entire avoidance responsibility to the controlled agent, which may produce oscillatory trajectories in dense multi-agent settings. Reciprocal velocity obstacles (RVO) address this limitation by symmetrizing avoidance responsibility and translating the forbidden velocity region so that both encountering agents share the obligation to yield, thereby suppressing oscillation [16]. Optimal reciprocal collision avoidance (ORCA) further approximates RVO cones using linear half-planes, converting the feasible velocity space into a convex polygon and enabling efficient optimization through quadratic programming [17]. Building on this cone-based formulation, subsequent studies extended the VO/RVO framework to interactive multi-agent navigation in crowded environments [18], cooperative avoidance for nonholonomic and kinematically constrained robots [19], and chance-constrained avoidance that explicitly accounts for motion and localization uncertainty [20], progressively broadening the applicability of velocity-space methods to more realistic multi-agent dynamic scenarios.

The basic VO principle is to identify all velocities that may result in collision. Using relative motion, it constructs an obstacle cone whose apex is associated with the relative velocity between the ownship and the obstacle and whose radius is determined by the safety distance. Its mathematical representation depends on their positions, velocities, and geometric envelopes, with the safety distance obtained by combining geometric radii and an additional safety margin. The method supports real-time collision avoidance with O(n) complexity, but has several limitations. It assumes that obstacles move at constant velocity along straight paths and is therefore less robust to maneuvering obstacles. Aircraft dynamic constraints are not inherently included, so the resulting velocities may be difficult to execute. Interacting avoidance actions among multiple aircraft may also create secondary collision risks, an issue also highlighted in studies on interactive multi-agent navigation [18].

Free-flight arrival systems have also been studied for vertiport operations [21]. RVO improves multi-aircraft coordination through reciprocal avoidance, assuming that obstacles

Just Accepted

follow the same type of avoidance strategy and adjusting relative-velocity weights. However, it does not account for airspace rules and is primarily applicable to unrestricted free flight. Its linear prediction of obstacle motion limits its response to abrupt maneuvers, and its single-objective velocity optimization does not explicitly balance trajectory smoothness and energy use. For ownship A and obstacle B, let their positions be p_A and p_B, their velocities be v_A and v_B, and their geometries be approximated by spheres of radii R_A and R_B, respectively. Define the relative velocity as $v_{AB} = v_A - v_B$. The collision cone is then given by:

$$CC_{AB} = \{v_{AB} | \text{ray} p_A + t v_{AB},\ t > 0, \text{intersects sphere B}\} \tag{1}$$

The velocity obstacle in absolute velocity space is consequently defined as:

$$VO_{AB} = \{v_A \mid v_A - v_B \in CC_{AB}\} \tag{2}$$

The ownship should select a velocity satisfying $v_A \notin \mathrm{VO}_{AB}$ to avoid collision. VO provides a fundamental geometric framework that maps obstacle positions and motion states into a velocity-space collision cone. A velocity inside this cone leads to collision under the model assumptions, whereas a velocity outside it permits collision-free motion. The cone is derived from obstacle geometry, such as circles or rectangles, and motion parameters, such as constant straight-line velocity, using relative kinematics. Specifically, for an ownship of radius r_A and a dynamic obstacle of radius r_B, the safety distance is defined as:

$$r_{safe} = r_A + r_B + \in \tag{3}$$

Here, ϵ is an additional safety margin. By computing the obstacle position and velocity relative to the ownship, VO constructs a conical region associated with the relative velocity and safety distance, converting spatial conflicts into velocity-space constraints.

Consider eVTOL aircraft A and B with radii R_A and R_B, positions and velocities P_A, P_B, v_A, and v_B, current time t, and control period T. The velocity obstacle for aircraft A relative to B can be defined as:

$$VO_A^B(v_B) = \{v_A \mid \lambda(P_A, v_A - v_B) \cap G\} \tag{4}$$

Here, $\lambda(P_A, v_A - v_B)$ is a ray originating at P in direction $v_A - v_B$, and G is the relative space in which aircraft A is represented as a point. To obtain the absolute-velocity representation for A, the VO region is translated by $|v_B|$ units in direction v_B, yielding $\mathrm{VO}_B^A(v_B)$, with boundaries v^{l} and v^{r}. This region contains the velocities at which aircraft A will collide with aircraft B within time T.

As illustrated in Fig. 1, extending VO to three-dimensional space replaces the planar circular aircraft representation with a sphere and the triangular velocity obstacle with a cone, yielding a three-dimensional velocity obstacle region.

Just Accepted

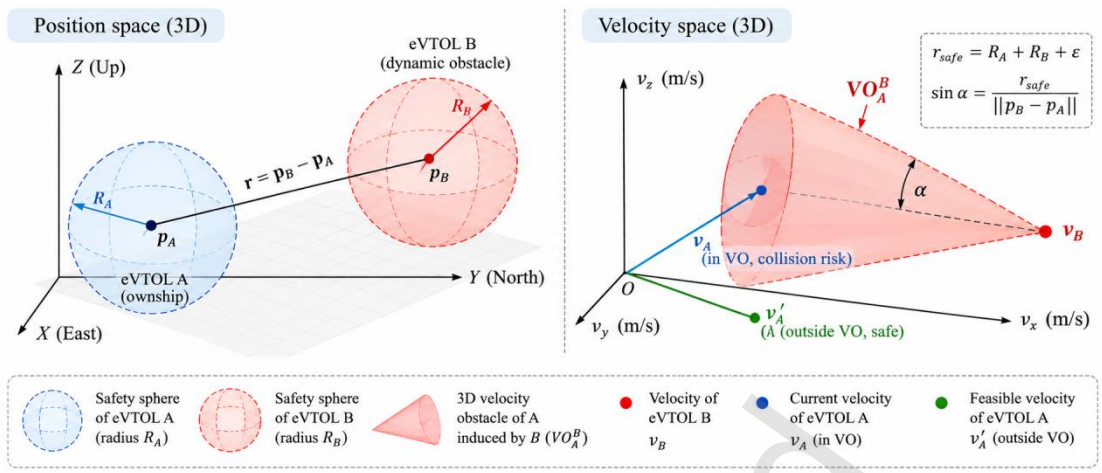


Fig. 1 Principle of the three-dimensional velocity obstacle (3D-VO) method.

VO offers low computational complexity, O(n) for n obstacles, and fast real-time responses. However, it is limited to obstacles moving at constant straight-line velocity, does not explicitly account for aircraft dynamic limits such as maximum speed and acceleration, and may produce secondary conflicts when several aircraft simultaneously avoid the same obstacle. To address these issues, van den Berg et al. proposed reciprocal velocity obstacles (RVO). When constructing the velocity obstacle, RVO considers both the ownship avoidance action and the assumption that the obstacle is also executing an avoidance strategy. Reciprocal adjustments are used to select velocities, and the obstacle boundary is modified through relative-velocity weights to coordinate multi-aircraft avoidance. For example, during a two-aircraft encounter, each aircraft may turn to its own right to avoid a head-on conflict, reducing the likelihood of conflicting avoidance actions. Although RVO outperforms VO in multi-aircraft free flight, it does not incorporate airspace rules, relies on linear obstacle-motion predictions, and focuses on collision avoidance rather than explicitly balancing smoothness and energy efficiency. Figure 2 compares simulated three-dimensional avoidance trajectories under different obstacle scenarios.

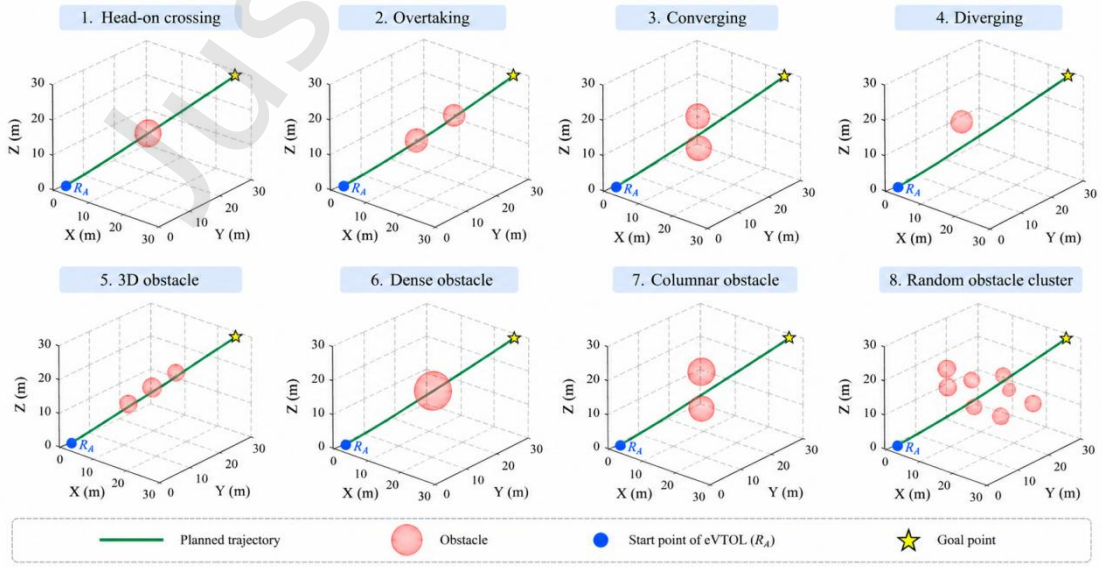


Fig. 2 Three-dimensional trajectories under different obstacle scenarios.

Just Accepted

1.1.2 Constrained Motion Planning

Motion planning is fundamentally an optimization problem in which a feasible trajectory must be found subject to multiple constraints. Depending on the constraints involved, it can be organized into three increasingly constrained levels: path planning, kinodynamic planning, and task-constrained motion planning [9]. Path planning considers collision avoidance and joint limits at the kinematic level, whereas kinodynamic planning additionally incorporates constraints such as velocity and acceleration. Task-constrained planning addresses requirements beyond collision avoidance, such as drawing along a surface or opening a drawer with a robotic manipulator. Conventional solution methods include sampling-based probabilistic roadmaps (PRM) and RRT, grid-based search, and APF. APF methods construct attractive potentials toward the goal and repulsive potentials around obstacles, providing computationally efficient real-time avoidance but remaining susceptible to local minima [22].

Constrained motion planning for complex dynamic systems such as eVTOL aircraft has received increasing attention. Heavy eVTOL aircraft have limited maneuverability in dense urban environments because of their large rotational inertia and actuator limits. Deep reinforcement learning methods can learn real-time collision-avoidance policies for resource-constrained robotic platforms [23,24]. Related eVTOL planning studies address energy–time trade-offs across city-scale wind fields [25] and health-aware operation under battery degradation [26]. Combining physical models with data-driven learning offers a means of handling complex dynamic constraints. Nevertheless, satisfying multiple constraints simultaneously while maintaining real-time performance in highly dynamic environments remains challenging.

1.1.3 Air-Ground Cooperative Systems

Air-ground cooperation is a representative form of heterogeneous robotic collaboration. It combines the broad field of view of unmanned aerial vehicles (UAVs) with the precise operation capabilities of unmanned ground vehicles (UGVs), with applications in search and rescue and autonomous exploration [5,6]. Such systems integrate aerial components, ground components, and supporting infrastructure: the aerial components include unobstructed flight corridors and airspace partitions, while the ground components include takeoff and landing facilities and loading stations [1]. This integrated architecture requires coordination among subsystems in perception, resource allocation, and task execution [2].

The evolution of autonomy in air-ground cooperation spans rule-driven coordination through emerging collective intelligence. Early work emphasized predefined coordination rules, such as communication protocols for yielding order and task allocation. More recent studies introduce deep learning and swarm intelligence to improve individual perception and decision-making and enable collective behavior. This research line also includes decentralized, non-communicating multiagent collision avoidance with deep reinforcement learning, in which offline training supports real-time local decisions [27,28]. Such methods motivate intention-aware coordination, although applying them to heterogeneous air–ground systems requires explicit interfaces for shared states and operational rules.

Just Accepted

Geometric methods provide efficient motion-level collision avoidance, constrained planning addresses trajectory generation under complex dynamic conditions, and air–ground cooperation integrates heterogeneous systems at the task level. Comparatively little work has explicitly embedded operational rules into a dynamic velocity obstacle framework to coordinate collision avoidance between eVTOL aircraft and ground infrastructure.

2 Problem Formulation

2.1 Problem Statement

This study considers autonomous eVTOL collision avoidance throughout a flight from a start point to a goal in an urban low-altitude environment. Three classes of environmental constraints are considered. Static obstacles include buildings, power transmission towers, and no-fly zones; their positions and geometry are obtained from prior models or onboard sensing. Dynamic obstacles include other eVTOL aircraft and UAVs, whose positions, velocities, and other motion states are obtained through inter-aircraft communication or perception. Operational rules include route networks, altitude allocations, and speed limits in structured airspace, defining the permitted motion space and operational boundaries.

The objective is to plan an optimal velocity vector in real time while satisfying aircraft kinematic limits, avoiding obstacles, and complying with operational rules, thereby reaching the goal safely and compliantly. Within a millisecond-level response budget, the planner must balance avoidance path length against acceleration and angular-rate limits. It must also incorporate airspace scheduling instructions and neighboring aircraft intention predictions, adjust trajectory curvature and climb rate, and generate continuous three-dimensional motion that satisfies minimum separation, no-fly-zone restrictions, and altitude-layer requirements at all times. The intended output is a verifiable control-command sequence compliant with DO-178C. To this end, a rule-constrained dynamic velocity vector optimization (RC-DVVO) framework is proposed.

Figure 3 illustrates autonomous eVTOL flight and conflict avoidance in UAM. The system response is divided chronologically into detection and tracking over T1, risk assessment over T2, and decision-making and path replanning over T3. After these stages, eVTOL 1 abandons its original dashed heading, which would lead to conflict, and follows a replanned path indicated by the curved solid arrow to avoid eVTOL 2. By using the vertical dimension, this strategy improves airspace utilization relative to conventional two-plane avoidance while maintaining smooth maneuvers and keeping the intruding aircraft outside the protection zone.

Just Accepted

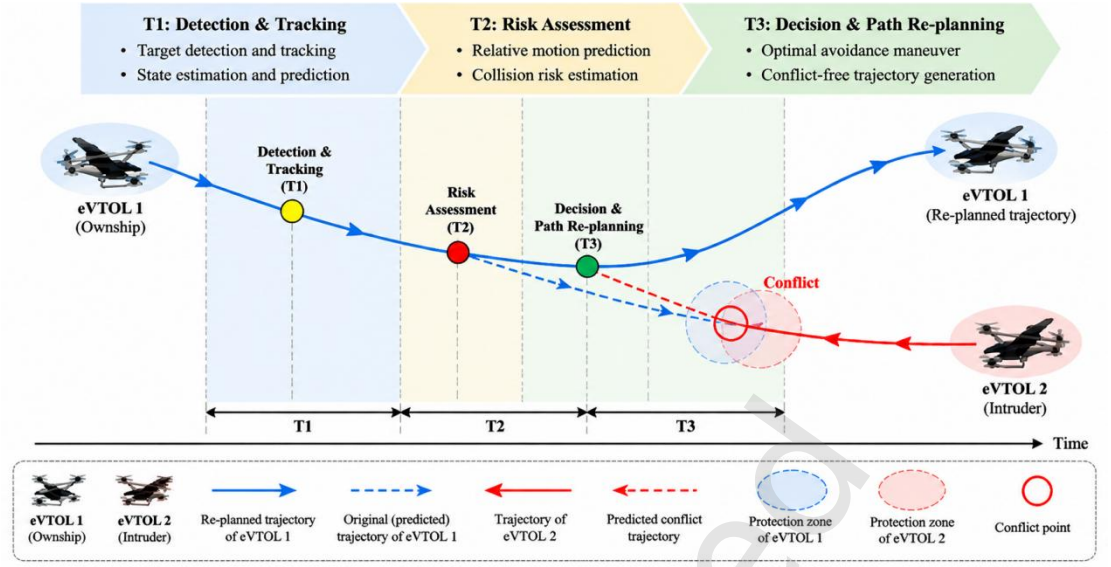


Fig. 3 Autonomous eVTOL flight and conflict avoidance.

2.2 Environmental Constraints

The three classes of environmental constraints are formalized as follows. The static obstacle set Ω_{static} includes buildings, power transmission towers, no-fly zones, and other fixed obstacles. Their geometry and spatial positions are obtained through prior modeling or onboard sensing and satisfy:

$$\Omega_{static} \subseteq R^3 \tag{5}$$

The dynamic obstacle set $\Omega_{\text{dynamic}}(t)$ includes other eVTOL aircraft, UAVs, and other moving aircraft. Their motion states are obtained through inter-aircraft communication or perception; their time-varying positions and velocities satisfy:

$$P_{dyn}(t) \in R^3, v_{dyn}(t) \in R^3 \tag{6}$$

The airspace operational rule set φ contains route-network, altitude-allocation, and speed-limit requirements in structured airspace. These define the permitted eVTOL motion space and are formalized as constraints on the feasible velocity domain:

$$v(t) \in \varphi(P(t), H(t), \theta(t)) \tag{7}$$

In Eq. (7), $P(t)$ denotes the three-dimensional eVTOL position at time t, $H(t)$ is the current altitude layer, and $\theta(t)$ is the set of permitted velocity directions in the current airspace. Following existing airspace classifications, a three-layer structured airspace model is established. The no-fly-zone layer represents prohibited regions, including government facilities, military restricted areas, and airport obstacle limitation areas, as polygonal prisms. The route-network layer defines fixed routes connecting sequences of waypoints; aircraft are expected to follow them unless deviations are authorized. The altitude-layer scheme assigns layers by flight direction and speed class, for example, 0–100 m for low-speed traffic, 100–200

Just Accepted

m for medium-speed traffic, and 200-300 m for high-speed traffic, with separation maintained among aircraft traveling in the same direction within a layer. Airspace rules can thus be expressed as feasible-velocity constraints:

$$v_{rule}(p) = \{v \in R^3 \mid p + v\Delta t \in F_{free}, v \in H(p), \| v \| \in [v_{\min}, v_{\max}]\} \tag{8}$$

Here, p is the current position, F_{free} is the free airspace, and $H(p)$ is the set of velocity directions permitted in the current altitude layer.

The following assumptions are adopted for the RC-DVVO model. Aircraft model: the eVTOL is treated as a rigid body in three-dimensional space, with position $p \in \mathbb{R}^3$ and velocity $V \in \mathbb{R}^3$. Its dynamics are simplified to velocity bounds $V_{\min} \le V \le V_{\max}$ and acceleration bounds $a_{\min} \le a \le a_{\max}$, and its geometry is approximated by a sphere of radius R or a cylinder–hemisphere combination. Obstacle model: dynamic obstacles have observable positions and velocities, and their short-term motion can be predicted using filtering. Static obstacles, including buildings and no-fly zones, have known positions and geometric boundaries and are modeled as convex polyhedra or cylinders. Perception and communication: onboard sensors provide ownship, neighboring aircraft, and environmental states in real time, subject to Gaussian white noise and a fixed delay. Inter-aircraft and air–ground communications are reliable within a specified range and support state and avoidance-intention exchange. Airspace rules: structured operational requirements are formalized as hard constraints, soft constraints, and discrete rules. Hard constraints include mandatory no-fly-zone restrictions and speed limits; soft constraints express preferences such as route-centerline tracking; discrete rules include logical requirements such as keeping right and priority-based yielding. These rules are provided in advance or updated in real time by the ground traffic management system.

The following coordinate frames are defined to describe aircraft motion and trajectory errors. The global frame F_G has its positive y-axis pointing north and its positive z-axis pointing upward. Heading is measured counterclockwise from the positive x-axis, so north corresponds to 90°. The climb angle is zero in the horizontal plane, positive for climbing, and negative for descending. In the body frame F_B, the positive x′-axis follows the horizontal velocity direction, the y′-axis is horizontal and perpendicular to x′, and the z′-axis is vertically upward and perpendicular to the x′–y′ plane. This frame describes the trajectory-error distribution. The dynamic obstacle plane (DA-Plane), spanned by relative position and relative velocity, is used to project three-dimensional avoidance into a two-dimensional problem and reduce computational complexity.

Let $\bar{p}(t)$ be the nominal UAV position in the global frame at time t and $\tilde{p}(t)$ its position error in the body frame. Assume that trajectory errors grow along the x_b, y_b, and z_b axes and are mutually independent. Then $\tilde{p} \sim N_3(0, \Lambda)$, and $\Lambda = \text{diag}(\sigma_1^2, \sigma_2^2, \sigma_3^2)$ is diagonal. Here, $\sigma_1^2, \sigma_2^2, \sigma_3^2$ denotes the variances along the three body-frame directions. The actual UAV position in the global frame is therefore given below, with t omitted for brevity:

$$\boldsymbol{r} = \boldsymbol{R}\tilde{\boldsymbol{p}} + \bar{\boldsymbol{p}} \tag{9}$$

Just Accepted

Here, R is the rotation matrix from the body frame to the global frame, calculated using Eq. (10):

$$\boldsymbol{R}(\theta,\varphi)=\begin{bmatrix}\cos\theta & -\sin\theta & 0\\ \sin\theta & \cos\theta & 0\\ 0 & 0 & 1\end{bmatrix}\begin{bmatrix}\cos\varphi & 0 & -\sin\varphi\\ 0 & 1 & 0\\ \sin\varphi & 0 & \cos\varphi\end{bmatrix}=\begin{bmatrix}\cos\theta\cos\varphi & -\sin\theta & -\cos\theta\sin\varphi\\ \sin\theta\cos\varphi & \cos\theta & -\sin\theta\sin\varphi\\ \sin\varphi & 0 & \cos\varphi\end{bmatrix} \tag{10}$$

Here, θ is the UAV heading and φ its climb angle. The actual position is therefore $r \sim N_3(\bar{p}, R\Lambda R^{\mathrm{T}})$. This model is intended for collision-avoidance decision analysis and uses simplified translational motion. It does not explicitly model coupling among attitude changes, aerodynamic forces, and actuator responses, and assumes that the low-level flight controller can track planned velocity commands within its operating envelope. The rigid-body assumption itself does not exclude external wind disturbances. Rather, the main simplification is that complex wind fields and their induced dynamic responses are not explicitly included in prediction and optimization. Model applicability consequently depends on whether actual tracking errors remain within the reserved safety margin; effectiveness under strong gusts or wind shear requires further validation.

2.3 Conflicts between Free-Flight Algorithms and Structured Airspace Rules

DVVO is a representative free-flight algorithm for autonomous eVTOL collision avoidance and offers real-time performance and local optimality in dynamic multi-obstacle scenarios. However, its original formulation targets unconstrained or weakly constrained free space, creating conflicts with structured UAM rules in four respects.

Decision objectives: DVVO is a local reactive approach that seeks collision-free motion, smooth trajectories, and low energy consumption. It considers current relative motion with neighboring aircraft and obstacles without accounting for global routes, flow allocation, or ground traffic scheduling. Structured airspace rules instead seek system-wide safety, compliant separation, orderly operations, and capacity. Aircraft must follow prescribed corridors, altitudes, and speeds rather than deviate arbitrarily, occupy conflicting channels, or maneuver frequently. In dense traffic, simultaneous locally optimal DVVO decisions can trigger cascading avoidance, intertwined paths, and oscillatory conflict resolution, reducing overall capacity and safety.

Constraint boundaries: DVVO considers geometric obstacles, safety distances, and dynamic limits but does not explicitly incorporate airspace regulations. Structured UAM requirements include airspace and no-fly/restricted-zone boundaries; altitude, speed, and heading ranges; turning and climb/descent limits; priority, keep-right, and heading-maintenance rules; and temporary ground instructions concerning flow restrictions and rerouting. Without recognizing these requirements, conventional DVVO may produce boundary incursions, speeding, prohibited turns, or priority violations, increasing operational and airworthiness-related risks.

Coordination architecture: DVVO generally uses distributed sensing and local decisions based on onboard sensors and inter-aircraft information exchange, without a closed loop with ground traffic management. UAM instead requires air–ground coordination: ground systems

Just Accepted

handle global planning, route allocation, strategic conflict resolution, and monitoring, while airborne systems perform local real-time avoidance and execute commands. Free-flight algorithms lack an interface for injecting ground rules and converting traffic-management requirements into computable constraints. Onboard actions can therefore conflict with ground scheduling intentions. Figure 4 illustrates air–ground cooperative conflict resolution for two eVTOL aircraft under structured airspace rules.

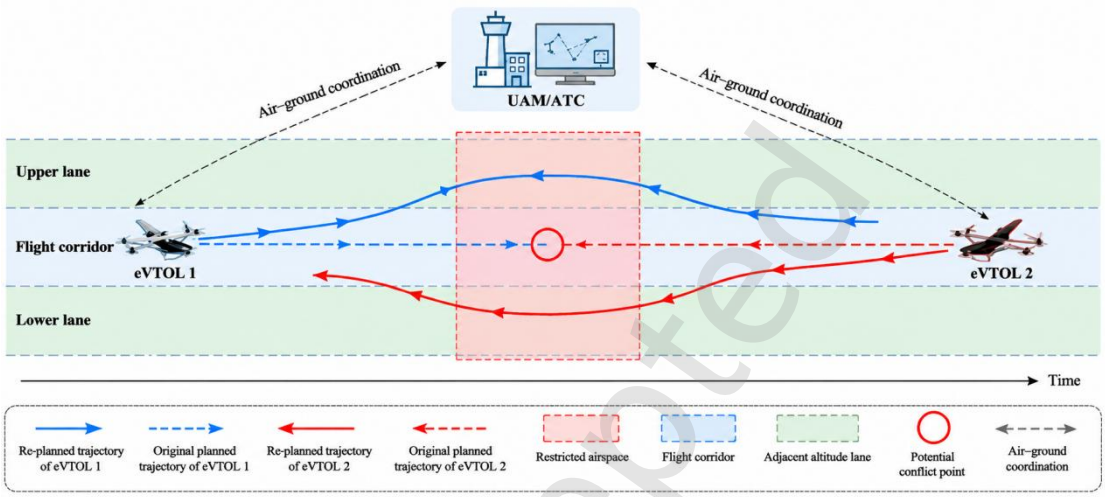


Fig. 4 Air-ground cooperative conflict resolution for two eVTOL aircraft.

Behavioral robustness: DVVO uses continuous convex optimization in velocity space to produce smooth velocity vectors, whereas airspace rules often introduce discrete, nonconvex, and sharply bounded constraints, such as fixed altitude layers, directional corridors, and prohibited crossings. Continuous optimization under nonconvex hard constraints may encounter empty feasible domains, oscillating solutions, and frequent switching. The resulting command discontinuities can impair stability and passenger comfort and, in extreme cases, cause loss of stability or secondary conflicts.

Conventional DVVO therefore has limitations in structured airspace, including incompatibility with operational rules, incomplete coordination loops, limited compliance guarantees, and insufficient robustness. Rule-aware and cooperative modifications are required to support safe, compliant urban low-altitude eVTOL operation. Operational rules and air-ground coordination must be systematically incorporated into the dynamic velocity obstacle framework to meet engineering and airworthiness requirements.

The RC-DVVO architecture comprises four modules. Environmental perception fuses observations from onboard cameras, lidar, and millimeter-wave radar with ground infrastructure such as 5G base stations and ADS-B to construct a local map and identify static and dynamic obstacles. Rule constraints are parsed from the current position and digital airspace map to generate the feasible velocity domain. Velocity optimization forms the algorithmic core and determines the optimal avoidance velocity within this domain. Air-ground coordination exchanges intentions with ground traffic management and neighboring aircraft to resolve conflicts cooperatively.

Just Accepted

3 Proposed Method

3.1 Feasible Velocity Domain Modeling for Structured Airspace Rules

For the structured urban low-altitude environment described above, operational rules are first converted from macroscopic traffic-management requirements into velocity constraints that can be incorporated into collision-avoidance decisions. Unlike unrestricted free flight, eVTOL operations in UAM must satisfy no-fly-zone restrictions, flight corridors, altitude layers, speed intervals, and traffic priorities in addition to avoiding static and dynamic obstacles. Rule modeling is therefore the first stage of RC-DVVO. A time-varying rule-feasible domain is constructed from the current position, altitude layer, and traffic situation, providing a compliant solution space for subsequent velocity obstacle modeling and optimization.

Let the ownship state at time t be (p_t, v_t), where $p_t = [x_t, y_t, z_t]^{\mathrm{T}}$ is the three-dimensional position and $v_t = [v_x, v_y, v_z]^{\mathrm{T}}$ the current velocity. Denote the structured airspace rule set by $R(t)$. The rule-induced feasible velocity domain is defined as:

$$V_R(t) = \{v \in \mathrm{R}^3 | v \text{ satisfies all operational rules at time } t\} \tag{11}$$

Following the structured airspace definition, the rules are divided into hard constraints, soft constraints, and discrete rule constraints. Hard constraints specify mandatory compliance boundaries: no-fly zones cannot be entered, corridor boundaries cannot be crossed, assigned altitude layers cannot be exceeded, and speed limits cannot be violated. Soft constraints describe preferred behavior, such as following the route centerline, maintaining the recommended heading, and returning toward the goal direction. Discrete rules describe logical requirements, including keeping right, priority-based yielding, and temporary ground instructions. The rule-feasible domain can thus be expressed as:

$$V_R(t) = V_H(t) \cap V_D(t) \tag{12}$$

Here, $V_H(t)$ is the strictly feasible domain defined by hard constraints, and $V_D(t)$ is the permissible velocity subdomain obtained by mapping discrete rules into logical constraints. Soft constraints do not directly prune velocity space; instead, they enter the optimization objective through a rule-recommended velocity $V_{\mathrm{rule}}(t)$. No-fly zones, corridors, and altitude layers are mapped jointly into a one-step position prediction constraint. Let the control period be Δt, the free airspace set be Ω_{free}, the altitude interval permitted in the current layer be $[z_{\min}(l_t), z_{\max}(l_t)]$, and the maximum speed allowed by the current rules be $v_{\max}(l_t)$. The hard constraints are then written as:

$$V_H(t) = \{v \mid p_t + v\Delta t \in \Omega_{free}, z_{\min}(l_t) \le z_t + v_z \Delta t \le z_{\max}(l_t), \| v \| \le v_{\max}(l_t)\} \tag{13}$$

This expression converts geographically defined rules into conditions that can be checked directly in velocity space. Discrete and region-based airspace requirements are thereby mapped into compliance boundaries for candidate velocity vectors and incorporated into local avoidance. Soft constraints guide velocity selection through preferences rather than directly excluding

Just Accepted

candidate velocities. Let $d_c(v)$ represent the route-centerline deviation cost for velocity v, $d_h(v)$ the target-heading deviation cost, and $d_s(v)$ the deviation cost relative to the recommended speed interval. The rule-recommended velocity is defined as:

$$\mathrm{v}_{rule}(t) = \arg\min_{v \in V_H(t)} (\lambda_1 d_c(v) + \lambda_2 d_h(v) + \lambda_3 d_s(v)) \tag{14}$$

Here, $\lambda_1, \lambda_2, \lambda_3$ denotes rule-preference weights. This formulation represents both prohibited actions and preferred behavior, providing directional guidance within the compliant domain for subsequent cooperative optimization.

Discrete rules are processed through logical evaluation, weight mapping, and velocity optimization. Mandatory requirements, including no-fly zones, assigned altitude layers, and required travel directions, are treated as hard constraints that prune the rule-feasible domain. Yielding preferences arising from mission priorities instead enter the objective through weight mapping. Let ownship and target-aircraft mission priorities be q_i and q_j, respectively, with $q_i, q_j \in \{1, 2, 3\}$; a larger value indicates higher priority. Define the relative yielding responsibility coefficient of the ownship as:

$$\rho_i = \frac{q_j}{q_i + q_j} \tag{15}$$

Here, $\rho_i \in (0, 1)$. When the target aircraft has higher mission priority, ρ_i increases, strengthening the ownship preference for yielding-compatible directions during candidate selection. When the ownship has higher priority, ρ_i decreases. For equal priorities or special traffic-management authorization, the actual avoidance direction remains governed by the applicable traffic rules and ground instructions.

Let D = {left turn, right turn, climb, descent, maintain heading} be the set of candidate maneuver directions. The score c(v) $\in$ [0, 1] measures how well the maneuver associated with candidate velocity v matches the current directional preference: c(v) = 1 indicates agreement and c(v) = 0 disagreement. Define the priority-dependent directional preference weight and discrete-rule cost as:

$$w(\rho_i) = w_0 + \alpha\rho_i \tag{16}$$

$$J_{disc}(v) = w(\rho_i)[1 - c(v)] \tag{17}$$

Here, $w_0 \geq 0$ is the base weight and $\alpha \geq 0$ the priority adjustment coefficient. To provide a reproducible initialization, $w_0 = 1$ and $\alpha = 2$ may be used as provisional values after all objective terms have been normalized; final values should be determined through weight-sensitivity tests. A candidate direction that clearly agrees with the preference is assigned c(v) = 1, and a direction that does not is assigned c(v) = 0. For continuous scoring, c(v) may be normalized to [0, 1] based on the angle between the candidate heading and recommended

Just Accepted

avoidance direction. These values are suggested initial settings and must be checked against the actual simulation implementation before being reported as experimental parameters.

In subsequent RC-DVVO optimization, $J_{\text{disc}}(v)$ is incorporated into the existing rule-guidance cost rather than weighted a second time. Among candidate velocities satisfying the rule-feasible, kinematically executable, and dynamic collision-free domains, the optimal velocity is selected using a composite cost containing $J_{\text{disc}}(v)$. Directional preference weights cannot replace mandatory rules. Velocities violating mandatory keep-right requirements, no-fly zones, or altitude restrictions must be removed from the feasible domain. Temporary ground instructions for rerouting, flow restrictions, or altitude occupancy update the rule set and directional compliance scores in real time, linking discrete logic to continuous velocity optimization. Figure 5 summarizes the mapping from structured airspace rules to feasible velocity domains and optimization preferences. First, the current state and traffic situation determine rule applicability and mandatory status. Spatial boundaries, speed limits, and mandatory discrete rules are mapped into computable constraints whose intersection defines the rule-feasible domain. Route tracking, recommended speed, and mission-priority preferences are then mapped into recommended velocities and associated costs. Together, these provide inputs for subsequent RC-DVVO optimization, allowing candidate selection to respect mandatory rules while considering operational preferences and further coupling with kinematic and dynamic avoidance requirements.

Just Accepted

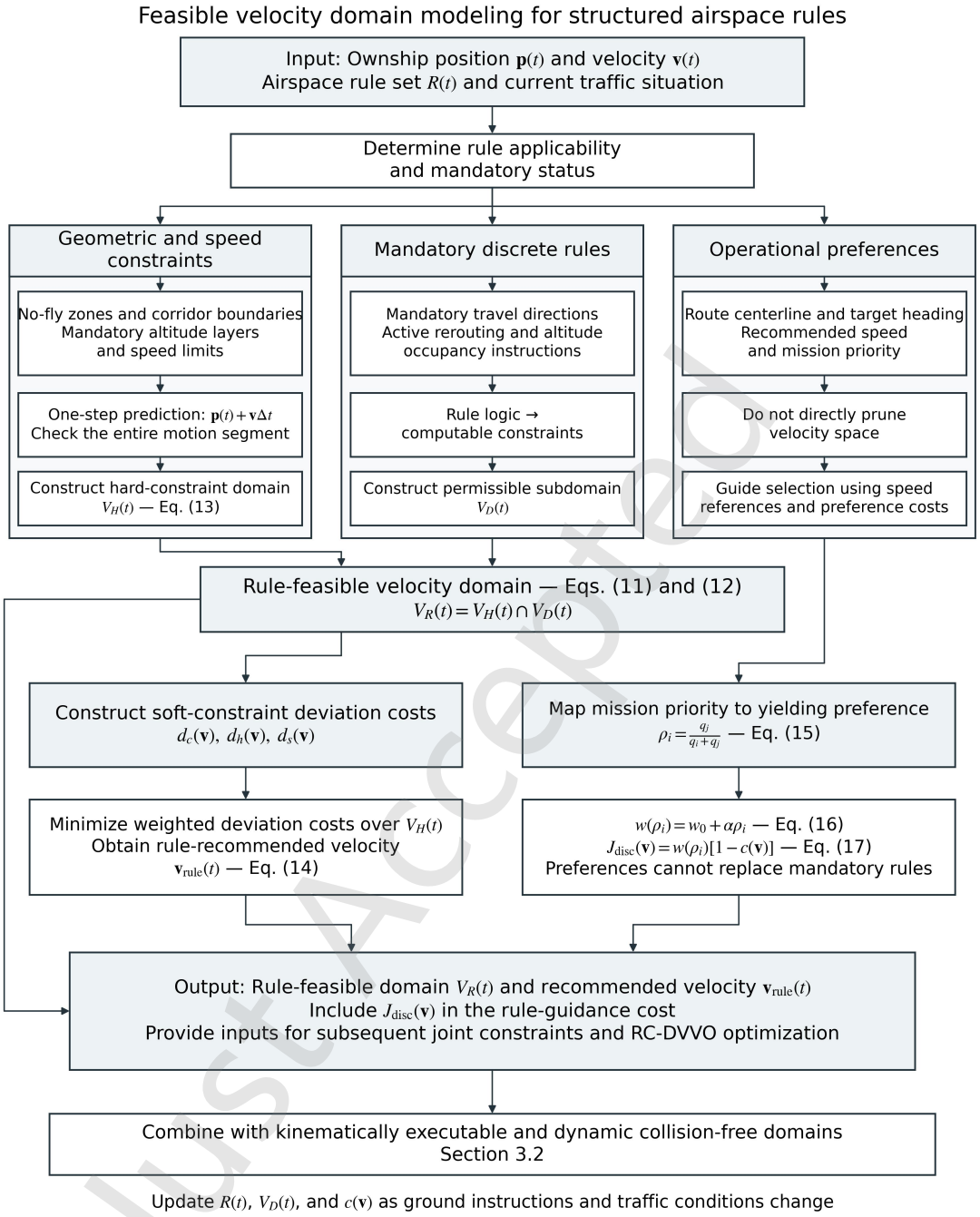


Fig. 5 Mapping structured airspace rules to feasible velocity domains and optimization preferences.

Rule-feasible domain modeling does not directly generate final control commands. Instead, it constructs a permitted velocity space by mapping operational rules into velocity constraints, establishing the basis for dynamic avoidance within compliance boundaries. Converting textual rules into velocity-space constraints enables conventional local avoidance algorithms to operate in structured airspace.

3.2 Construction of the Rule-Constrained Dynamic Velocity Vector Optimization Model

After constructing the rule-feasible domain, the remaining task is to avoid dynamic obstacles within that permitted velocity space. Operational constraints and dynamic prediction

Just Accepted

are therefore incorporated into conventional VO to construct the RC-DVVO model. The central idea is to combine the forbidden velocities arising from dynamic obstacles with the rule-feasible and kinematically executable domains, jointly representing compliance, safety, and executability in velocity space. Denote the dynamic obstacle set by $O(t) = \{o_1, o_2, ..., o_n\}$. For obstacle o_j, let its current state be $(p_{j,t}, v_{j,t})$ and the required ownship-obstacle separation be $d_{\text{safe},j}$. In the conventional VO framework, if a future instant $\tau \in (0, T)$ exists at which the relative distance falls below the safety separation when the ownship travels at velocity v, then v belongs to the collision-velocity set. The velocity obstacle associated with o_j is defined as:

$$VO_j(T) = \{v \in R^3 \mid \exists \tau \in (0,T), \| p_{j,t} - p_t + (v_{j,t} - v)\tau \| \leq d_{safe,j}\} \tag{18}$$

Urban low-altitude obstacles may accelerate, turn, or maneuver vertically. A short-term motion prediction model is therefore introduced, replacing constant-velocity extrapolation with the predicted trajectory p_j(τ). The dynamic velocity obstacle is constructed as:

$$DVO_j(T) = \{v \in R^3 \mid \exists \tau \in (0,T), \| \hat{p}_j(\tau) - (p_t + v\tau) \| \leq d_{safe,j}\} \tag{19}$$

The region $\text{DVO}_j(T)$ contains candidate velocities that may lead to collision within prediction horizon T. A velocity inside it indicates a future collision risk under the current decision; a velocity in its complement satisfies the basic geometric safety conditions over that horizon. Conventional DVVO generally performs local optimization based only on geometric safety. Here, the rule-feasible domain $V_R(t)$ and kinematically executable domain $V_{\text{kin}}(t)$ are additionally incorporated, yielding the overall feasible velocity set of RC-DVVO:

$$V_F(t) = V_{kin}(t) \cap V_R(t) \cap (R^3 \setminus \cup DVO_j(T)) \tag{20}$$

Here, $V_{\text{kin}}(t)$ is the set of velocities permitted by the aircraft kinematics, including maximum level-flight speed, acceleration, angular rate, and climb/descent-rate limits. Equation (20) indicates that RC-DVVO does more than add a rule penalty to conventional VO. It reconstructs velocity space through the intersection of three constraint classes: $V_R(t)$ enforces rule compliance, $V_{\text{kin}}(t)$ enforces physical executability, and $R^3 \setminus \cup DVO_j(T)$ enforces dynamic collision avoidance. Only velocities in their intersection are candidates for optimization. The trajectory-error and coordinate-transformation models established above are further used to represent uncertainty in RC-DVVO risk assessment. Position uncertainty for the ownship and dynamic obstacles is projected onto the DA-Plane using the body-frame error distribution and its global-frame transformation. An analytical trajectory-error propagation method is then used to obtain the relative-position distribution and estimate collision probability under candidate velocity v. Let the collision probability associated with obstacle O_j be $p_j(v)$. Then:

$$p_j(v) = \Pr\left(\min_{\tau \in (0,T)} \| p(\tau) - p_j(\tau) \| \leq d_{\text{safe},j}\right) \tag{21}$$

Just Accepted

Here, $p(\tau)$ and $p_j(\tau)$ are the random actual positions of the ownship and obstacle aircraft, respectively, after trajectory errors are included. This probabilistic risk representation extends deterministic geometric avoidance to probabilistic safety assessment and improves robustness to perception noise, communication delays, and maneuver uncertainty.

RC-DVVO is thus a rule-constrained dynamic velocity optimization model that jointly uses dynamic velocity obstacles and probabilistic risk assessment to constrain candidate velocities within rule-feasible and kinematically executable domains, then outputs an optimal velocity vector through real-time optimization. Relative to conventional DVVO, it explicitly incorporates structured airspace rules, uses dynamic prediction and probabilistic risk modeling to improve responses to noncooperative maneuvering obstacles, and integrates compliance, collision avoidance, and executability in one velocity space to support efficient online solution. In Fig. 6, the cost surface exhibits pronounced ridges and high-cost regions, shown as white/red peaks, indicating candidate velocities with elevated risk or rule-deviation costs under the simulated conditions. RC-DVVO filters and optimizes candidates using the rule-feasible domain, kinematic domain, and dynamic avoidance constraints to seek a lower-cost avoidance velocity. These results characterize optimization under the specified airspace boundaries, obstacle states, and prediction horizon. Safety remains dependent on estimation errors, obstacle maneuvers, and the availability of feasible velocities.

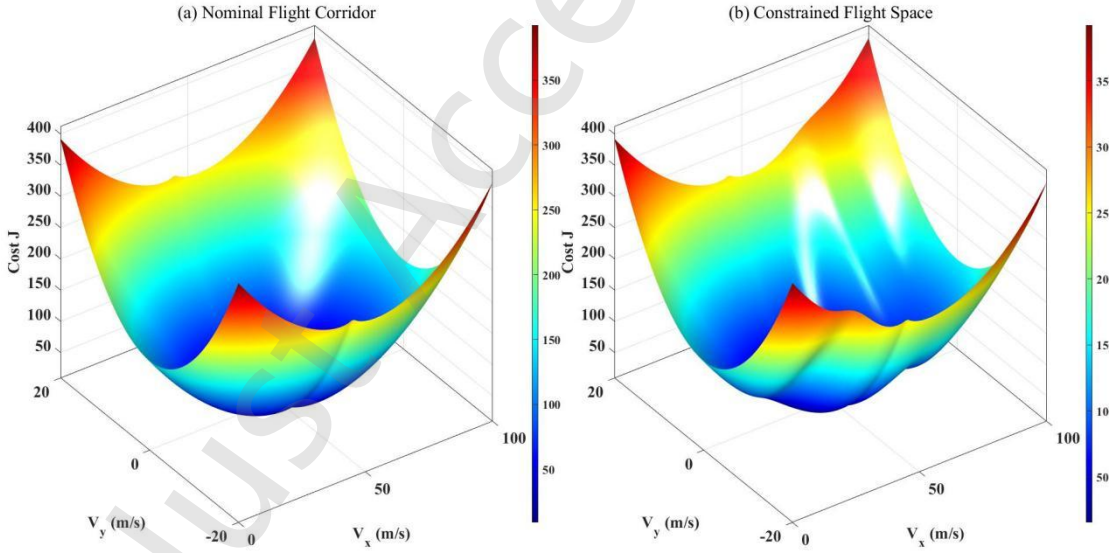


Fig. 6 Analysis of rule-constrained dynamic velocity obstacle avoidance.

3.3 Multi-objective Velocity Optimization and Real-Time Solution under Air-Ground Coordination

Equation (20) defines candidate velocities satisfying rule, avoidance, and dynamic constraints. In operation, however, this set generally contains more than one velocity. A final selection must balance goal progress, compliance, risk reduction, maneuver smoothness, and cooperative consistency. A cooperative optimization model is therefore constructed over $V_F(t)$, incorporating ground-system information and neighboring aircraft intentions to solve for the velocity in real time under air–ground coordination.

Just Accepted

Define the goal-guidance velocity as $v_g(t)$, directed toward the current mission goal or local reference waypoint, and denote the rule-recommended velocity from Eq. (14) by $v_{\text{rule}}(t)$. To balance safety, compliance, and efficiency, the following objective is constructed:

$$J(v) = w_1 \| v - v_g(t) \|^2 + w_2 \| v - v_{rule}(t) \|^2 + w_3 \sum_{j \in O(t)} \phi_j(v) + w_4 \| v - v_{t-1} \|^2 + w_5 C_{\text{int}(v)} \tag{22}$$

The first term promotes progress toward the mission goal. The second is the rule-guidance term, penalizing corridor-centerline deviations, inappropriate headings, and unsuitable speed choices. The third is a risk term that penalizes candidate velocities approaching dynamic obstacles or collision boundaries. The fourth promotes smoothness by limiting velocity changes between consecutive control cycles, improving trajectory continuity and passenger comfort. The fifth is a cooperation term that combines neighboring aircraft intentions and ground scheduling information to reduce cascading conflicts caused by locally optimal decisions. The risk term $\phi_j(v)$ jointly incorporates collision probability and time to collision:

$$\phi_j(v) = \alpha p_j(v) + \beta \exp\left(-\frac{\tau_j(v)}{k}\right) \tag{23}$$

Here, $p_j(v)$ is the collision probability in Eq. (21), $\tau_j(v)$ is the predicted time to collision with obstacle o_j under candidate velocity v, and α, β and k are risk adjustment parameters. This formulation considers both collision likelihood and urgency and is intended to reflect dynamic risk more fully than geometric distance or TTC alone. Intention consistency is introduced into the cooperation term to represent air–ground and inter-aircraft coordination. Let the neighboring aircraft set be $N(t)$, the predicted intention velocity broadcast by aircraft k be $v_k^{\text{int}}(t)$, and the ground-recommended control velocity be $v_{\text{gnd}}(t)$. The cooperation term is defined as:

$$C_{\text{int}}(v) = \sum_{k \in N(t)} \eta k \| v - v_k^{\text{int}}(t) \|^2 + \eta g \| v - v_{gnd}(t) \|^2 \tag{24}$$

Here, η_k and η_g are the neighboring-aircraft and ground-coordination weights, respectively. When conflicts intensify ahead, corridor capacity is constrained, or temporary rerouting or speed instructions are issued, this term aligns onboard decisions with system-wide scheduling rather than relying only on the ownship perspective. In addition to the feasible velocity set in Eq. (20), dynamic and safety-boundary constraints are imposed. Let the maximum acceleration be $a_{\max}$, maximum angular rate be $\varphi_{\max}$, maximum climb/descent rate be $z_{\max}$, minimum permissible time to collision be $\tau_{\min}$, and maximum permissible collision probability be p. The cooperative optimization problem is then expressed as:

Just Accepted

$$
\begin{aligned}
&\min J(v)\\
&s.t. v \in V_F(t),\\
&\| v - v_{t-1} \| \le a_{\max}\Delta t,\\
&|\phi(v)| \le \phi_{\max},\\
&|v_z| \le z_{\max},\\
&p_j(v) \le p, \forall j \in o(t),\\
&\tau_j(v) \ge \tau_{\min}, \forall j \in o(t)
\end{aligned}
\tag{25}
$$

As illustrated in Fig. 7, planning with constraints on the energy-consumption distribution, heading, and safety-risk field improves overall flight efficiency.

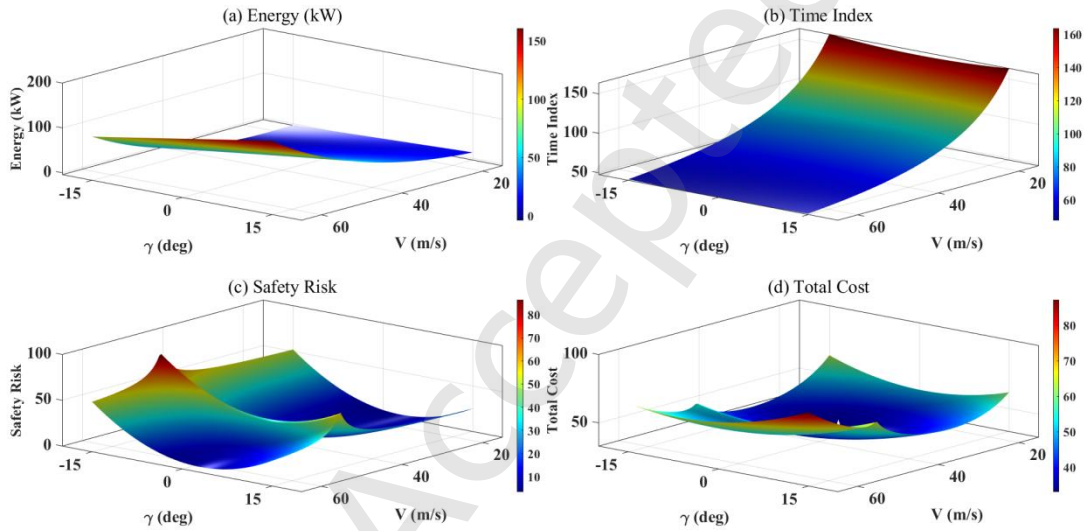


Fig. 7 Comparison of physical constraints in motion planning.

Equation (25) constitutes the final cooperative optimization model. Unlike conventional VO, which selects velocities only from the geometric collision-free complement, the objective explicitly balances goal progress, rule compliance, risk reduction, intention coordination, and smoothness. Its constraints jointly enforce compliance, dynamic executability, and predicted safety.

To meet onboard real-time requirements, a solution strategy combining rule-based pruning, risk assessment, and local continuous optimization is used. During each control cycle, $V_R(t)$ is first updated using the current position, digital airspace map, and ground rules. Dynamic obstacle states are then predicted from fused sensing and inter-aircraft communication to construct $\mathrm{DVO}_j(T)$. Candidate velocities are generated within $V_F(t)$ and optimized locally using Eqs. (22)–(25). Finally, the optimal command $v^*(t)$ is sent to the low-level flight controller, while the ownship intention is broadcast to neighboring aircraft and the ground system. This closes the loop through rule parsing, obstacle prediction, feasible-domain generation, risk assessment, cooperative optimization, intention exchange, and control execution. Figure 8 illustrates avoidance under the cooperative objective. When obstacles 1 and 2 create a narrow passage, cooperative planning guides the eVTOL safely through it toward the goal.

Just Accepted

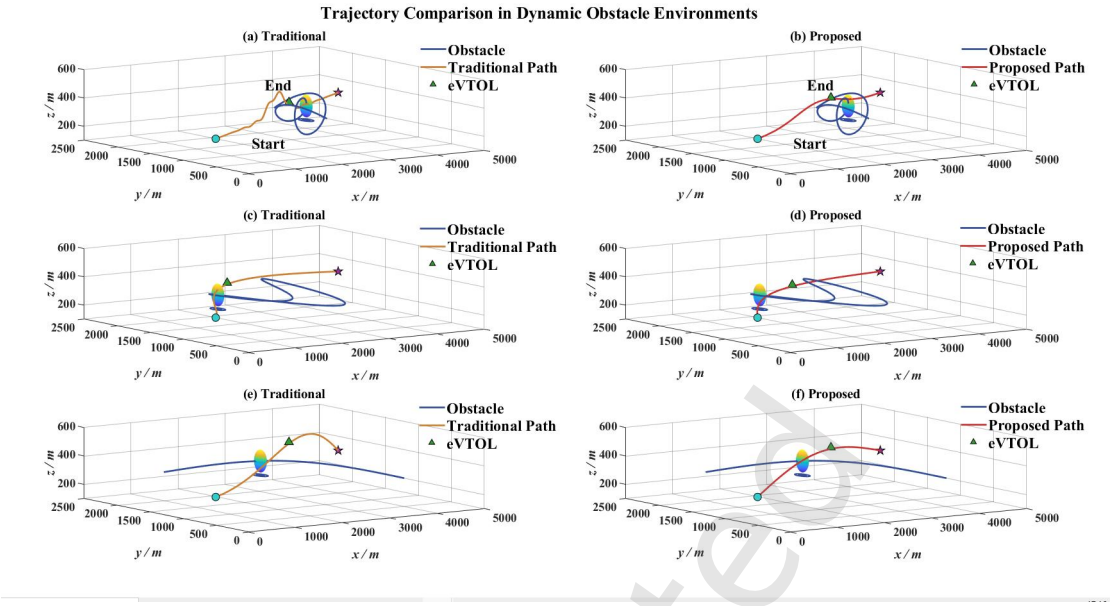


Fig. 8 Collision avoidance under the cooperative optimization objective.

RC-DVVO is implemented jointly by airborne and ground components. The airborne component performs environmental perception, local risk assessment, candidate generation, and rapid optimization to provide millisecond-level avoidance responses. The ground component maintains airspace rules, manages traffic flows, resolves conflicts strategically, and issues temporary instructions to maintain orderly operations. Their bidirectional information exchange supports Eqs. (24) and (25), aligning local autonomous avoidance with macroscopic traffic organization.

The proposed model and solution strategy connect rule space, velocity obstacle space, and optimal control space in a closed loop. The resulting velocity vector balances compliance, collision safety, smoothness, and cooperative consistency. The rule-feasible domain reduces violations; the risk function and dynamic prediction improve avoidance success and robustness; continuous velocity optimization and smoothing improve trajectory curvature; and local velocity optimization in place of receding-horizon trajectory optimization supports 20 Hz decisions.

4 Simulation Results and Discussion

4.1 Simulation Setup

The environmental layer uses real urban geographic information extracted from OpenStreetMap (OSM) to build a three-dimensional digital twin of a 1 km × 1 km × 300 m central business district in a major city. The scene contains 127 static obstacles, including buildings, roads, tower cranes, and power lines, together with designated no-fly zones, restricted areas, and flight corridors. The perception layer simulates an onboard sensor suite comprising a camera with 1920 × 1080 resolution at 30 Hz, 32-channel lidar with a 100 m range and ±2 cm accuracy, millimeter-wave radar with a 150 m range and ±0.1 m/s velocity accuracy, and an ADS-B In receiver updating at 1 Hz. Gaussian white noise and delay models approximate sensor characteristics. The decision layer implements RC-DVVO and the baseline

Just Accepted

algorithms and outputs desired velocity vectors to the low-level flight controller at 20 Hz. The evaluation layer records trajectories, decision times, and conflict events for offline analysis.

Simulations were performed on a desktop computer with an Intel Core i5-11400F processor, 16 GB RAM, and an NVIDIA GeForce GT 710 graphics card with 2 GB video memory, running a 64-bit Windows operating system and MATLAB R2024b. A simulation environment incorporating structured airspace rules, dynamic obstacles, and aircraft kinematic limits was developed to compare classical DVVO, APF, rule-constrained model predictive control (RC-MPC), and the proposed RC-DVVO.

To compare computational efficiency fairly, all algorithms use the same scenarios, control frequency, and evaluation criteria. Each collision-avoidance decision is treated as one timing sample. The time required to evaluate candidate velocities and output a decision for the current state is recorded, and the mean and standard deviation are calculated. The control frequency is 20 Hz, corresponding to a 50 ms cycle, against which decision times are assessed.

(1) Scenario configuration: a typical urban canyon is formed by two parallel tall buildings, with a virtual one-way flight corridor 30 m wide and 50 m high between them. A static cylindrical no-fly zone represents a temporary facility. The ownship eVTOL flies from the corridor start to its endpoint.

(2) Dynamic threat: a small UAV intruder enters laterally at a random time with a random speed and direction, representing an unplanned dynamic obstacle.

(3) Baselines: three methods are selected to evaluate RC-DVVO. Classical DVVO relies only on geometric collision avoidance and does not incorporate operational rules. APF combines goal attraction and obstacle repulsion, representing corridor boundaries as repulsive fields without systematic rule handling. RC-MPC embeds airspace rules as constraints in a nonlinear MPC formulation and performs receding-horizon optimization.

(4) Performance metrics: collision-avoidance success rate is the proportion of cases in which obstacles are avoided without collision. Rule-violation rate is the proportion of flight trajectories crossing corridor boundaries or entering no-fly zones. Mean computation time is the average duration of a decision cycle in milliseconds. Trajectory smoothness is measured by the root mean square (RMS) of acceleration changes. Mission completion time is the total time from start to goal. Figure 9 shows the spatiotemporal evolution of rule-constrained autonomous eVTOL avoidance from t = 0.0 s to 15.0 s. The trajectories of eVTOL 1 and eVTOL 2 are shown as blue and red solid lines, respectively; their original trajectories are dashed. Dynamic obstacles are shown as gray disks with surrounding safety regions. Light-red shading indicates restricted airspace, while light-blue shading marks the flight corridor, illustrating how the aircraft adjust their velocity vectors to maintain separation while following cooperative rules.

Just Accepted

Table 1 Simulation parameters and uncertainty test settings.

Category	Parameter	Symbol	Value	Unit
Basic parameters	Flight corridor width	W_c	30	m
Basic parameters	Maximum eVTOL speed	v_{max}	15	m/s
Basic parameters	Maximum eVTOL acceleration	a_{max}	3	m/s²
Basic parameters	Dynamic inflation margin	d_{exp}	1.5	m
Control parameters	Control frequency	f_c	20	Hz
Communication parameters	Typical communication delay	τ_c	100	ms
Perception uncertainty	Position noise (low)	σ_{pos}	0.2	m
Perception uncertainty	Position noise (medium)	σ_{pos}	0.5	m
Perception uncertainty	Position noise (high)	σ_{pos}	1.0	m
Perception uncertainty	Velocity noise (low)	σ_{vel}	0.1	m/s
Perception uncertainty	Velocity noise (medium)	σ_{vel}	0.2	m/s
Perception uncertainty	Velocity noise (high)	σ_{vel}	0.4	m/s
Communication uncertainty	Communication delay (typical/high)	τ_c	100 / 200	ms
Obstacle motion uncertainty	Obstacle acceleration	a_o	±2	m/s²
Obstacle motion uncertainty	Heading change rate	$\dot{\psi}_o$	±10	°/s
Statistical settings	Monte Carlo runs (baseline evaluation)	N_{MC}	100	—
Statistical settings	Runs per uncertainty combination	N_{rob}	50	—

Just Accepted

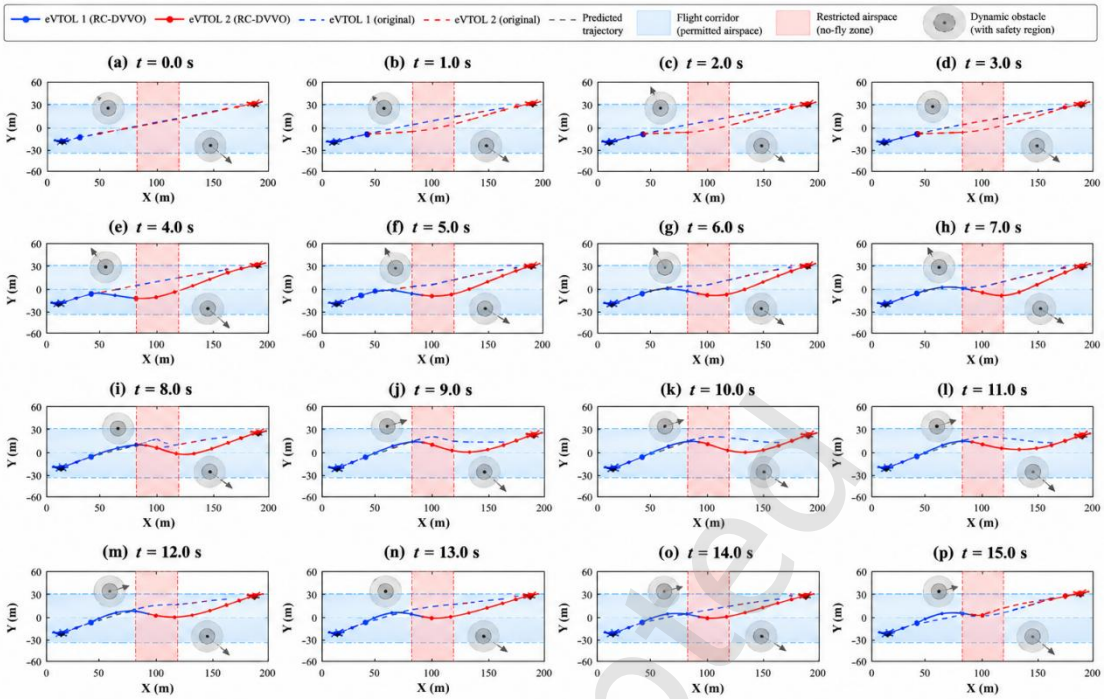


Fig. 9 Spatiotemporal evolution of eVTOL autonomous collision avoidance under rule constraints.

Classical DVVO, APF, RC-MPC, and RC-DVVO use the same simulation scenarios, initial states, dynamic-obstacle motions, airspace boundaries, and evaluation metrics. Aircraft kinematic limits, safety separation requirements, simulation time steps, and control update frequencies are also identical to reduce the effects of external experimental differences.

The main parameters are configured and calibrated according to each algorithm. For classical DVVO, these include prediction horizon, safety separation, and candidate-velocity sampling resolution. APF parameters include attractive and repulsive gains and potential-field influence range. RC-MPC parameters include prediction and control horizons, state and control weights, and solver termination conditions. RC-DVVO parameters include rule-constraint weights, dynamic-obstacle prediction horizon, and candidate-velocity optimization settings. They should be selected according to the principles of each method, common safety requirements, and preliminary experiments.

To avoid underestimating baseline performance through unsuitable parameter choices, calibration should use independent preliminary experiments or sensitivity tests. Parameter combinations should be assessed jointly using success rate, rule violations, smoothness, and computation time. Once selected, parameters remain fixed throughout the formal comparison and are not adjusted for individual test cases. Repeated simulations under common scenarios and metrics are used to characterize mean performance and variability, reducing the influence of parameter selection and experimental differences.

4.2 Test Scenarios

Basic compliant avoidance: two parallel buildings, each 120 m tall and separated by 40 m, form an urban canyon. A virtual corridor 30 m wide and 50 m high represents a one-way route in structured UAM airspace. A cylindrical no-fly zone of radius 5 m and height 30 m is placed

Just Accepted

on the centerline to represent a temporary facility or sensitive area. The ownship flies from (0 m, 0 m, 25 m) to (200 m, 0 m, 25 m), complying with corridor boundaries and no-fly-zone restrictions throughout. At t = 15 s, a noncooperative UAV enters from the right at 90° and 10 m/s, crossing the corridor perpendicularly and creating an encounter with the ownship.

Dense multi-obstacle conflicts: two additional static obstacles representing building protrusions are placed on opposite sides of the 30 m corridor at (80 m, ±8 m, 20–40 m), leaving a passage only 14 m wide. Between t = 10 s and 25 s, three dynamic obstacles enter sequentially from different directions. The first enters from the left at 45° and 8 m/s, the second from the right at 30° and 12 m/s, and the third descends vertically from above at 6 m/s. This represents dense heterogeneous traffic.

Uncertainty robustness: Monte Carlo experiments evaluate sensitivity to perception noise, communication delay, and uncertain obstacle motion. Three noise levels are used: low (position noise $\sigma_{\text{pos}} = 0.2$ m and velocity noise $\sigma_{\text{vel}} = 0.1$ m/s), medium ($\sigma_{\text{pos}} = 0.5$ m and $\sigma_{\text{vel}} = 0.2$ m/s), and high ($\sigma_{\text{pos}} = 1.0$ m and $\sigma_{\text{vel}} = 0.4$ m/s). Communication delays are 100 ms, representing typical 4G/5G delay, and 200 ms, representing severe congestion. Obstacle motion comprises constant straight-line velocity, constant acceleration of ±2 m/s², and random disturbances with heading-rate changes of ±10°/s. Fifty independent runs are performed for each parameter combination to obtain performance distributions.

Air-ground cooperative avoidance under temporary ground instructions: an additional experiment introduces temporary airspace-control instructions into the dynamic-obstacle scenario to evaluate rule response and autonomous avoidance under air–ground coordination. It examines whether the airborne algorithm can update constraints promptly after the ground management system issues an instruction and replan using predicted dynamic-obstacle motion.

The aircraft parameters remain unchanged: maximum speed 15 m/s, maximum acceleration 3 m/s², control frequency 20 Hz, and typical communication delay 100 ms. At a preset time, the ground management system temporarily closes a local airspace region, providing its spatial boundaries and effective time. Upon reception, the airborne system maps the new restriction into velocity space, updates the rule-feasible domain, and reconstructs the dynamic velocity obstacle using the intruder's short-term predicted trajectory.

Two groups, with and without the temporary instruction, are compared. They have identical initial positions, flight speeds, obstacle motion, and algorithm parameters; only reception and execution of the temporary restriction differ. With the instruction, RC-DVVO reselects candidates using the updated rule-feasible, kinematically executable, and dynamic collision-free domains, then generates an adjusted trajectory through velocity vector optimization.

The spatial trajectories, minimum dynamic-obstacle separation, incursions into the temporary restricted region, mission completion time, path length, and instruction-response time are recorded for both groups. Comparing trajectories before and after the instruction takes effect characterizes decisions under simultaneous dynamic avoidance and temporary airspace constraints, providing further simulation evidence for the air–ground coordination mechanism.

Just Accepted

4.3 Quantitative Performance Comparison

Table 2 summarizes 100 Monte Carlo runs for this scenario. One-way analysis of variance (ANOVA) with Tukey's honestly significant difference (HSD) post hoc test is used to assess performance differences at a significance level of $\alpha = 0.05$.

Collision-avoidance success rate: both RC-DVVO and RC-MPC achieve 99%, significantly higher than classical DVVO at 94% ($p < 0.01$) and APF at 91% ($p < 0.001$). Of the six classical DVVO failures, four involve near-boundary collision risk within 1 m of the no-fly zone. Although no physical collision occurs, these are classified as failures under the strict safety criterion. The remaining two result from insufficient avoidance caused by intruder-velocity estimation errors. Of the nine APF failures, seven involve prolonged hovering at local minima followed by collision with subsequent obstacles, while two involve oscillatory instability caused by unsuitable potential-field parameters.

Rule-violation rate: RC-DVVO achieves 0.8%, significantly below classical DVVO at 7.2% ($p < 0.001$) and APF at 4.5% ($p < 0.001$), with no significant difference from RC-MPC at 1.1% ($p = 0.23$). These results indicate that incorporating rules as feasible-domain constraints improves compliance. RC-DVVO violations occur mainly while returning to the centerline after avoidance, when a strong goal-guidance term produces brief approaches to the boundary. Further tuning of the weight k_goal may improve this behavior.

RC-DVVO failures and potential mechanisms: the 99% success rate indicates safe avoidance in most tested conditions, although a small number of cases fail the predefined safety criterion. Several potential causes follow from dynamic prediction and constraint coupling. First, abrupt obstacle acceleration or heading changes, combined with sensing noise and communication delay, may cause predicted trajectories to differ from actual motion, so the dynamic velocity obstacle does not fully represent the true risk. Second, dense multi-obstacle encounters can substantially shrink the intersection of rule-feasible, kinematically executable, and dynamic collision-free domains; in extreme cases, the local feasible velocity set may be empty. Finally, acceleration limits and finite control cycles may leave insufficient maneuver time after an obstacle enters close proximity, even if the risk is correctly detected.

Computational efficiency: RC-DVVO has a mean decision time of 12.3 ms with a standard deviation of 1.5 ms, significantly below RC-MPC at 28.6 ms ($p < 0.001$) and of the same order as classical DVVO at 8.5 ms and APF at 5.2 ms. Direct velocity-space optimization avoids MPC's receding-horizon trajectory-optimization overhead and supports the 20 Hz onboard embedded-control requirement of no more than 50 ms per decision. The decision-time breakdown attributes 35% to rule-feasible domain construction, 42% to avoidance-cone computation, and 23% to optimization.

Trajectory smoothness: RC-DVVO has a mean curvature of 0.0132 rad/m, significantly lower than classical DVVO at 0.0185 rad/m ($p < 0.001$), APF at 0.0221 rad/m ($p < 0.001$), and RC-MPC at 0.0154 rad/m ($p < 0.05$). Continuous velocity-space optimization generates smooth velocity profiles and reduces repeated turns near hard boundaries and potential-field oscillations. Curvature peaks for RC-DVVO occur primarily at the beginning and end of avoidance, whereas classical DVVO maintains higher curvature throughout. Figure 10 compares the two methods

Just Accepted

quantitatively. RC-DVVO yields the lowest mean curvature, below the stated comfort threshold of 0.02 rad/m, indicating improved flight smoothness. During the main avoidance phase, optimized maneuvers reduce curvature substantially and suppress severe oscillation.

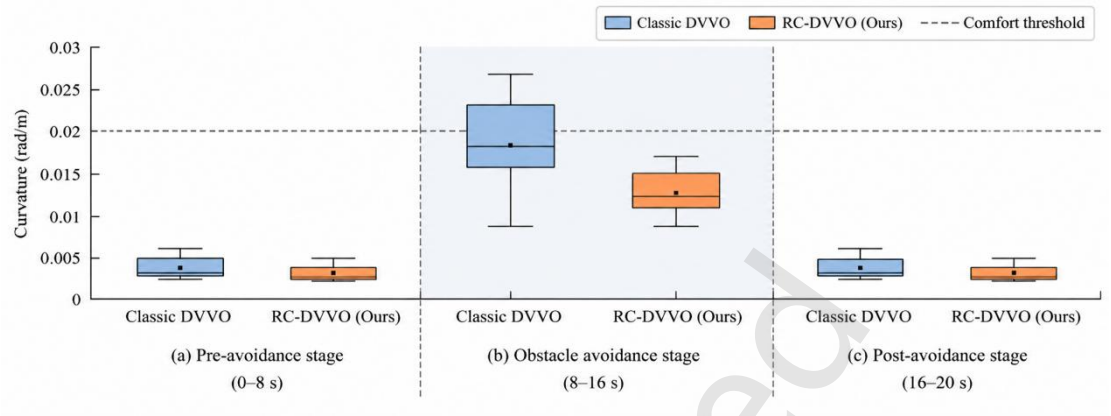


Fig. 10 Curvature comparison between classical DVVO and RC-DVVO.

Mission completion time: RC-DVVO at 21.8 s does not differ significantly from classical DVVO at 21.3 s ($p = 0.18$). Both are faster than APF at 23.7 s ($p < 0.001$) and RC-MPC at 22.1 s ($p < 0.05$). Thus, introducing operational rules does not significantly compromise path efficiency, and cooperative optimization balances safety, compliance, and efficiency.

The response to a single dynamic intrusion is examined in detail. At t = 15 s, the intruding UAV enters from the right, corresponding to the positive y direction, at 10 m/s and a heading of 0°, perpendicular to the corridor. It is predicted to meet the ownship near the centerline at t = 17.2 s, with a minimum geometric distance of 0.8 m, creating a severe collision risk.

Three phases are defined: perception from t = 15.0–15.2 s, avoidance decision and maneuvering from t = 15.2–18.5 s, and recovery after t = 18.5 s.

Classical DVVO: after detecting the intruder at t = 15.1 s, the algorithm constructs a velocity obstacle cone and chooses a direction that moves the relative velocity outside it. Because its sole objective is to minimize target-heading deviation, it turns slightly left and forward, changing heading by +12°, to pass behind the intruder as quickly as possible. It avoids collision with a minimum separation of 6.2 m, but the trajectory deviates substantially from the centerline and crosses the right corridor boundary over x = 95–115 m, with a maximum deviation of 4.2 m. After avoidance, the aircraft returns toward the centerline at the maximum turning rate, producing an abrupt recovery and a curvature peak of 0.035 rad/m.

APF: modeling corridor boundaries as repulsive fields creates a force toward the centerline and partially limits the flight region. However, when obstacle and boundary repulsion oppose one another, the resultant direction changes sharply, causing oscillations near the boundary. The heading-rate standard deviation during avoidance reaches 8.5°/s, higher than for the other methods. APF also becomes trapped in a local minimum over t = 16.8–17.5 s, hovering and oscillating for approximately 0.7 s before escaping, which increases mission time.

RC-MPC: embedding rules as hard constraints keeps predicted trajectory points within corridor boundaries and outside no-fly zones. Upon detecting the intruder, RC-MPC plans a moderate right-forward deviation that maintains a minimum separation of 7.1 m while

Just Accepted

remaining within the corridor. However, solving a nonlinear optimization problem at each decision instant imposes greater computation, with a mean decision time of 28.6 ms. Optimization near hard boundaries also produces boundary-hugging trajectories, increasing local curvature to a peak of 0.022 rad/m.

RC-DVVO: this method provides the best overall performance. After sensing the intruder at t = 15.1 s, it queries the digital airspace map at the current position and constructs rule constraints that prevent crossing the corridor boundary, $|y| \leq 15$ m, or entering the no-fly region, $x \in [80, 120]$ m and $|y| \leq 5$ m. It then constructs the dynamic velocity obstacle and solves the objective in Eq. (25). The selected maneuver turns 15° right and forward at 9.8 m/s, maintaining a minimum separation of 6.8 m and remaining inside the corridor with a maximum deviation of only 1.2 m. After avoidance ends at t = 18.3 s, goal guidance returns the aircraft smoothly to the centerline without oscillation or overshoot; peak curvature is only 0.016 rad/m. Figure 11 compares the four methods using success rate, rule-violation rate, mean computation time, trajectory smoothness, mission completion time, and path length. Original metrics and units are retained without reciprocal transformations or cross-metric normalization. Higher success rates indicate better avoidance; lower violation rates, computation times, curvature, completion times, and path lengths indicate better compliance, computational efficiency, smoothness, and mission efficiency, respectively. Means and standard deviations are listed in Table 2. RC-DVVO performs well in success rate, compliance, and smoothness, while requiring less computation than RC-MPC, demonstrating favorable overall performance.

Table 2 Quantitative performance comparison in Scenario 1 (mean ± standard deviation).

Algorithm	**Avoidance success (%)**	**Rule violations (%)**	**Mean decision time (ms)**	**Trajectory smoothness (rad/m)**	**Mission time (s)**	**Path length (m)**
Classical DVVO	94±2.1	7.2±1.3	8.5±1.2	0.0185±0.0021	21.3±0.8	212.5±3.2
APF	91±3.2	4.5±1.8	5.2±0.9	0.0221±0.0034	23.7±1.2	226.8±4.5
RC-MPC	99±1.1	1.1±0.4	28.6±3.5	0.0154±0.0018	22.1±0.6	216.3±2.1
RC-DVVO	99±1.0	0.8±0.3	12.3±1.5	0.0132±0.0015	21.8±0.5	214.2±1.8

Just Accepted

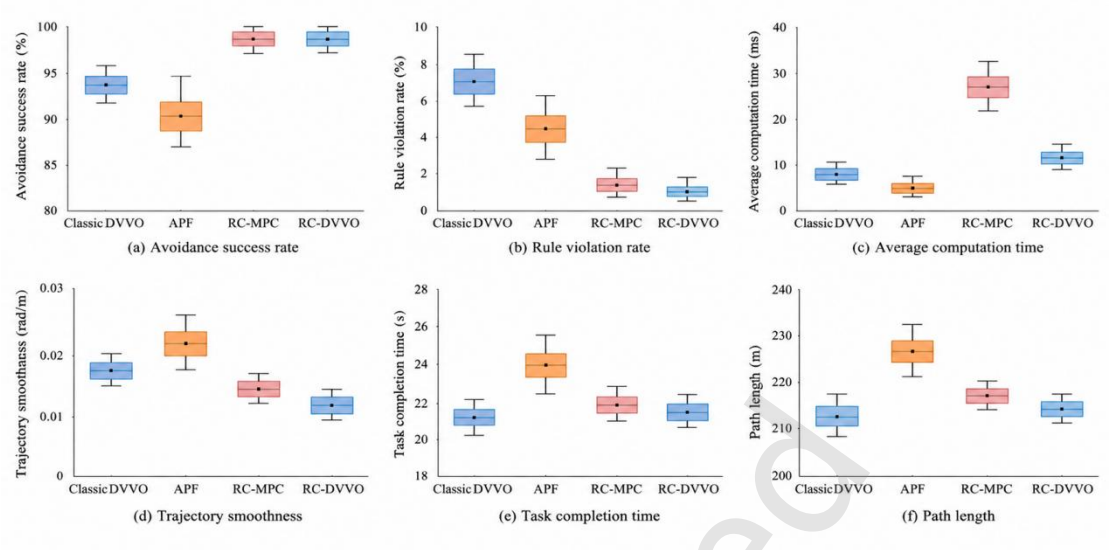


Fig. 11 Comprehensive performance comparison of RC-DVVO and benchmark collision-avoidance algorithms.

4.4 Applicability and Limitations under Complex Disturbances

RC-DVVO primarily addresses local avoidance in structured urban low-altitude airspace. Its effectiveness depends on timely updates of ownship and obstacle states, some short-term predictability of obstacle motion, and low-level flight-control capability sufficient to track planned commands. The simulations consider perception noise, communication delay, and uncertain obstacle motion, but do not explicitly model complex urban-canyon wind fields or full six-degree-of-freedom dynamics. The findings therefore cannot be directly generalized to strong gusts, wind shear, or other extreme weather.

Complex wind fields can affect avoidance through velocity-tracking errors, accumulated position-prediction errors, and inaccurate safety-boundary estimates. Gusts or local airflow changes may cause actual velocity to depart from the planned value, accumulating position errors over the prediction horizon. These alter relative positions, relative velocities, and time to collision, potentially causing the dynamic velocity obstacle constructed from nominal states to underestimate risk. Near narrow corridors or no-fly zones, lateral drift or altitude errors may push actual trajectories across safety boundaries even when nominal predictions satisfy the rules. Persistent wind disturbances may also consume control authority, making commands deemed feasible under nominal velocity and acceleration limits difficult to execute.

The Gaussian-error and directional-independence assumptions also limit applicability. Urban-canyon winds may exhibit temporal correlation, directional coupling, and abrupt changes. Retaining a fixed error distribution may therefore underestimate the probability of large deviations. Abrupt maneuvers, close-range intrusions, or several obstacles simultaneously constraining a corridor can combine prediction errors with insufficient remaining maneuver time. The intersection of the rule-feasible, kinematically executable, and dynamic collision-free domains may then shrink or become empty. Periodic replanning can correct decisions using updated states, but does not establish safety guarantees under disturbances of arbitrary magnitude.

Just Accepted

Future work should incorporate aircraft-specific dynamics, wind resistance, and control-response characteristics into wind estimation and disturbance prediction, and investigate separation expansion and rule-boundary contraction as prediction uncertainty changes. Coupled wind-field and six-degree-of-freedom simulations, hardware-in-the-loop testing, and controlled flight experiments are needed to establish applicability under different disturbances. If disturbances exceed the validated operating envelope or the local feasible velocity set is empty, an independent operational safety mechanism should initiate mission termination, rerouting, diversion, or other appropriate action.

5 Conclusions

This study proposes a rule-constrained dynamic velocity obstacle framework, RC-DVVO, for autonomous eVTOL collision avoidance in complex structured urban low-altitude airspace. Operational rules are converted into feasible-velocity constraints to jointly optimize compliance and dynamic obstacle avoidance. The main contributions and findings are summarized below.

A mathematical representation of structured airspace rules is established. No-fly zones, route networks, and altitude layers are formalized as feasible-velocity constraints, converting discrete regulatory boundaries into constraints that can be incorporated into continuous optimization. Hard constraints, soft constraints, and discrete logical rules are defined, together with a mechanism for dynamically constructing the rule-feasible domain. A rule-constrained dynamic velocity obstacle model is then developed. Operational constraints are incorporated into conventional VO to jointly address compliance and avoidance. A risk function and a trajectory-error-based collision-probability method, UPTE, extend deterministic geometry to probabilistic assessment. Under the modeled rule, kinematic, and dynamic avoidance conditions, candidates are screened and optimized jointly to improve compliance and avoidance capability. Actual safety still depends on complete constraint modeling, accurate state estimates, and reliable obstacle predictions. Continuous velocity-space optimization produces smooth, executable commands.

An air-ground cooperative mechanism enables intention exchange and conflict resolution between eVTOL aircraft and ground traffic management, extending distributed autonomous decisions to cooperative operation. Ground systems provide airspace rules and traffic information, while aircraft upload states and intentions. Bidirectional exchange coordinates global scheduling with local avoidance and reduces cascading maneuvers and conflict oscillations in dense traffic. Three-dimensional simulations based on real urban geographic information evaluate multiple dynamic obstacles and scenario complexities with sensing noise, communication delay, and obstacle-motion uncertainty. In the basic compliant-avoidance scenario, RC-DVVO achieves a 99% success rate, a 0.8% violation rate, and a trajectory-smoothness value of 0.0132 rad/m, improving on classical DVVO in avoidance, compliance, and trajectory quality. In dense multi-obstacle conflicts, it maintains a 95% success rate and 1.4% violation rate, compared with 82.7% and 13.8% for classical DVVO. Monte Carlo uncertainty experiments indicate the lowest sensitivity to noise, delay, and obstacle maneuvers among the compared methods and smaller performance degradation, attributed to probabilistic risk modeling and intention exchange. Ablation experiments attribute an 84.7%

Just Accepted

reduction in violations to rule constraints, an 11.8% success-rate improvement to the risk function, and a 5.1% success-rate gain to intention exchange; probabilistic modeling improves robustness to perception uncertainty.

Across all scenarios, RC-DVVO improves success rate over classical DVVO by an average of 12.6 percentage points, reduces rule violations by 84.7%, shortens paths by 4.2%, and achieves a mean curvature of 0.0128 rad/m. The mean decision time of 12.3 ms remains well within the 50 ms budget required for 20 Hz onboard control. These results support integrating rule constraints into velocity obstacle methods and provide a methodological basis for safe eVTOL operation in low-altitude intelligent networks. The conclusions are limited to the simplified motion model and specified simulations; avoidance under strong gusts, wind shear, and other complex weather has not been validated. Future work will combine wind estimation, dynamic constraints, and adaptive safety margins to determine the method's operational limits in complex urban low-altitude environments.

Funding

This research was funded by the Major Project of the National Social Science Fund of China (No. 22&ZD169) and the Key Program of the Civil Aviation Joint Fund of the National Natural Science Foundation of China (Nos. U2133207 and U2333214).

Declaration of competing interest

The authors have no competing interests to declare that are relevant to the content of this article.

Author contribution statement

Yuetan Zhang conceived the study, drafted the manuscript and performed the analysis. Honghai Zhang supervised the research and revised the manuscript. Wei Pan and Yulin Yuan assisted with data sorting and literature collation.

Data availability statement

The data supporting the findings of this study are available from the corresponding author upon reasonable request.

Use of AI statement

No AI tools were utilized for this manuscript. All work was performed independently by the authors, who are responsible for the content.

Just Accepted

References

[1] Straubinger A, Rothfeld R, Shamiyeh M, et al. An overview of current research and developments in urban air mobility-setting the scene for UAM introduction. Journal of Air Transport Management, 2020, 87: 101852.

[2] Badea C. Conflict detection and resolution for constrained urban airspace. Doctoral thesis. Delft: Delft University of Technology, 2025. https://doi.org/10.4233/uuid:5d40d6b6-7ac3-49c3-9fa4-e8858b6db451.

[3] Weinert A, Campbell S, Vela A, et al. Well-clear recommendation for small unmanned aircraft systems based on unmitigated collision risk. Journal of Air Transportation, 2018, 26(3): 113-122. https://doi.org/10.2514/1.D0091.

[4] Weng C, Chen C, Tan J, et al. Real-time traffic simulation and management for large-scale urban air mobility: Integrating route guidance and collision avoidance. arXiv preprint, 2024, arXiv:2412.01235. https://doi.org/10.48550/arXiv.2412.01235.

[5] Li Z, Mao R, Chen N, et al. ColAG: A collaborative air-ground framework for perception-limited UGVs' navigation. arXiv preprint, 2023, arXiv:2310.13324. https://doi.org/10.48550/arXiv.2310.13324.

[6] Yue P, Xin J, Huang Y, et al. UAV autonomous navigation system based on air–ground collaboration in GPS-denied environments. Drones, 2025, 9(6): 442. https://doi.org/10.3390/drones9060442.

[7] Rodionova A, Pant YV, Jang K, et al. Learning-to-Fly: Learning-based collision avoidance for scalable urban air mobility. arXiv preprint, 2020, arXiv:2006.13267. https://doi.org/10.48550/arXiv.2006.13267.

[8] Panchal I, Armanini SF, Metz IC. Validation of collision detection and avoidance methods for urban air mobility through simulation. arXiv preprint, 2023, arXiv:2311.18047. https://doi.org/10.48550/arXiv.2311.18047.

[9] Kingston Z, Moll M, Kavraki LE. Sampling-based methods for motion planning with constraints. Annual Review of Control, Robotics, and Autonomous Systems, 2018, 1: 159-185.

[10] Marchidan A, Bakolas E. Collision avoidance for an unmanned aerial vehicle in the presence of static and moving obstacles. Journal of Guidance, Control, and Dynamics, 2019, 42(1): 96-110.

[11] Choi M, Rubenecia A, Shon T, et al. Velocity obstacle based 3D collision avoidance scheme for low-cost micro UAVs. Sustainability, 2017, 9(7): 1174. https://doi.org/10.3390/su9071174.

[12] Huang Y, Chen L, van Gelder PHAJM. Generalized velocity obstacle algorithm for preventing ship collisions at sea. Ocean Engineering, 2019, 173: 142-156.

[13] Bertram J, Wei P, Zambreno J. A fast Markov decision process-based algorithm for collision avoidance in urban air mobility. IEEE Transactions on Intelligent Transportation Systems, 2022, 23(9): 15420-15433. https://doi.org/10.1109/TITS.2022.3140724.

[14] Bertram J, Zambreno J, Wei P. Efficient unmanned aerial systems navigation with collision avoidance in dense urban environments. IEEE Transactions on Intelligent Transportation Systems, 2023, 24(8): 8163-8173. https://doi.org/10.1109/TITS.2023.3281131.

[15] Fiorini P, Shiller Z. Motion planning in dynamic environments using velocity obstacles. The International Journal of Robotics Research, 1998, 17(7): 760-772.

[16] van den Berg J, Lin M, Manocha D. Reciprocal velocity obstacles for real-time multi-agent navigation. Proceedings of the 2008 IEEE International Conference on Robotics and Automation, 2008: 1928-1935.

[17] van den Berg J, Guy SJ, Lin M, et al. Reciprocal n-body collision avoidance. Robotics Research: The 14th International Symposium ISRR. Springer, 2011: 3-19.

[18] van den Berg J, Patil S, Sewall J, et al. Interactive navigation of multiple agents in crowded environments. Proceedings of the 2008 ACM SIGGRAPH Symposium on Interactive 3D Graphics and Games. ACM, 2008: 139-147.

Just Accepted

[19] Alonso-Mora J, Beardsley P, Siegwart R. Cooperative collision avoidance for nonholonomic robots. IEEE Transactions on Robotics, 2018, 34(2): 404-420.

[20] Zhu H, Alonso-Mora J. Chance-constrained collision avoidance for MAVs in dynamic environments. IEEE Robotics and Automation Letters, 2019, 4(2): 776-783.

[21] Waltz M, Okhrin O, Schultz M. Self-organized free-flight arrival for urban air mobility. arXiv preprint, 2024, arXiv:2404.03710. https://doi.org/10.48550/arXiv.2404.03710.

[22] Khatib O. Real-time obstacle avoidance for manipulators and mobile robots. The International Journal of Robotics Research, 1986, 5(1): 90-98.

[23] Diao X, Wang J. Efficient multi-agent navigation with lightweight DRL policy. arXiv preprint, 2024, arXiv:2408.16370v1. https://arxiv.org/abs/2408.16370v1.

[24] Schulman J, Levine S, Abbeel P, et al. Trust region policy optimization. Proceedings of the 32nd International Conference on Machine Learning. PMLR, 2015: 1889-1897.

[25] Liu S, Li S, Li H, et al. TEeVTOL: Balancing energy and time efficiency in eVTOL aircraft path planning across city-scale wind fields. arXiv preprint, 2024, arXiv:2403.14877. https://doi.org/10.48550/arXiv.2403.14877.

[26] Montazeri M, Kulkarni C, Fink O. Prescribing optimal health-aware operation for urban air mobility with deep reinforcement learning. arXiv preprint, 2024, arXiv:2404.08497. https://doi.org/10.48550/arXiv.2404.08497.

[27] Chen YF, Liu M, Everett M, et al. Decentralized non-communicating multiagent collision avoidance with deep reinforcement learning. Proceedings of the 2017 IEEE International Conference on Robotics and Automation. IEEE, 2017. https://doi.org/10.1109/ICRA.2017.7989037.

[28] Zhang Yuetan, Zhang Honghai, Tang Weibin, Pan Wei, Zhang Chenfeng, Dai Caiyu, Yuan Yulin. Research on Collision Avoidance Methods for Logistics Unmanned Aerial Vehicle Based on Dynamic Controlled Interactive Collaborative Fusion. Journal of Field Robotics, 2026. https://doi.org/ 10.1002/rob.70219.

Author biography



Yuetan Zhang is a Ph.D. candidate at Nanjing University of Aeronautics and Astronautics. His research focuses on risk avoidance in autonomous air-ground collaborative operations of low-altitude aircraft, safety governance of low-altitude traffic systems, and intelligent collaborative control mechanisms in low-altitude airspace. He has edited two textbooks, including Logistics Drone Operation and Maintenance (Advanced), received four awards at provincial/municipal levels and above, published eight papers in key journals, and filed 10 invention patents.



Honghai Zhang is Vice Dean, Professor, and Ph.D. Supervisor, and Deputy Director of the State Key Laboratory of Air Traffic Management System. He leads a CAAC key innovation team. He has undertaken six national and 48 provincial/ministerial research projects and received 10 ministerial-level science and technology awards.

Just Accepted